THE JOURNAL OF PHYSICAL CHEMISTRY LETTERS
A JOURNAL OF THE AMERICAN CHEMICAL SOCIETY

pubs.acs.org/JPCL

Letter

Spectroscopic Characterization of the Synergistic Mechanism of Ruthenium−Lithium Hydrides for Dinitrogen Cleavage

Jumei Zhang, Gang Li, Jianping Guo, Hongjun Fan, Ping Chen, Ling Jiang,* and Hua Xie*

Cite This: J. Phys. Chem. Lett. 2022, 13, 3937−3941

Read Online

ACCESS | Metrics & More | Article Recommendations | Supporting Information

ABSTRACT: Elucidating the role of alkali/alkaline earth metal hydrides in dinitrogen activation remains an important and challenging goal for spectroscopic studies of bulk systems, because their spectral signatures are often masked by the collective effects. Herein, mass-selected photoelectron velocity-map imaging spectroscopic and quantum chemical calculation techniques are utilized to explore the promotion mechanism of LiH in the Ru-based catalysts toward N_2 activation. The $RuHN_2^-$ anion is determined to be a N_2-tagged complex. In contrast, the $RuHN_2(LiH)_n^-$ (n = 1 and 2) anions are characterized to have N≡N bond-cleaved ring structures. These observations indicate that the complexation of LiH to RuH^- significantly facilitates N≡N bond cleavage. Theoretical analyses show that the synergy between Ru and LiH efficiently lowers the energy barrier of N≡N bond cleavage. These findings clarify the pivotal roles played by the LiH species in the transition metal catalysts for N_2 activation and have important practical implications for the prospective design of high-performance catalysts via metal tuning strategies.

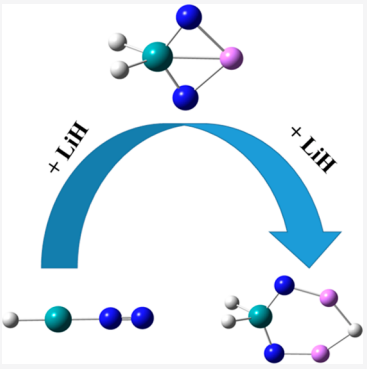

The conversion of N_2 into NH_3 is vital for the production of nitrogen fertilizers and the utilization of NH_3 as a carbon-free energy or hydrogen carrier.[1] However, current industrial ammonia production via the conventional Haber−Bosch process requires harsh operating conditions (673−773 K, 100−300 bar), which actually constitutes >1% of the world's annual energy production. The efficient activation and transformation of dinitrogen under mild conditions is one of the formidable challenges in chemistry and has been actively pursued for more than a century.[2−6] The reduction of N_2 to NH_3 is generally mediated by transition metals because they possess unoccupied and occupied d orbitals with suitable orbital energies and symmetries, which can bind to N_2 via synergistic σ donation and π back-donation.[7−9] Transition metal−nitrogen interactions play an important role in catalytic ammonia production, which can be seen as the initial step of the complex sequential chemical activation of dinitrogen.

In general, the synthesis of ammonia requires the dissociative chemisorption of nitrogen and hydrogen molecules to generate surface nitrogen atoms and hydrogen atoms, followed by sequential hydrogenation of surface nitrogen atoms to produce NH, NH_2, and NH_3.[10−12] The reaction rate of ammonia synthesis is closely related to the dissociation of N_2. An ideal catalyst for mild-condition ammonia synthesis should have a strong activation of the N_2 molecule but weak adsorption of the intermediate NH_x species. However, it is difficult to achieve simultaneous synthesis of ammonia on a single transition metal surface.[13−17]

Alkali and alkaline earth metals are electron-rich and have easy access to high-energy orbitals and the correct symmetry to interact effectively with the π^* orbital of N_2. Hence, they usually serve as the promoters for ammonia catalysts to increase the N_2 dissociation rate.[18−24] The alkali and alkaline earth hydrides (denoted as AMHs) feature a negatively charged hydrogen atom, which can be regarded as an electron and hydrogen carrier by abstracting and hydrogenating the dissociated N from the transition metals. The synergy between alkali or alkaline earth metal hydrides and transition metals allows both early and late 3d TM−AMH composites to exhibit superior mild-condition catalytic activities.[25] Gas-phase cluster investigations have revealed that a series of complex hydride clusters such as $[Li_4FeH_6]^-$ and $[Li_5FeH_7]^-$ are identified upon bombarding the Fe−LiH composite catalyst, which can undergo a stoichiometric reaction with dinitrogen to form NH_2-containing clusters.[26] The Ru−LiH composite catalyst works as an efficient catalyst for mild-condition ammonia synthesis from N_2 and H_2.[27] This synergy between the transition metal and LiH has created a favorable pathway to allow transition metal−LiH composites for N_2 activation and hydrogenation to NH_3.[13,25,26] However, a molecular-level understanding of the role of alkali and alkaline earth metal hydrides in N_2 activation remains elusive. Herein, we perform photoelectron velocity-map imaging spectroscopy on mass-selected $RuHN_2(LiH)_n^-$ (n = 0−2) as models to explore the

Received: March 12, 2022
Accepted: April 25, 2022

https://doi.org/10.1021/acs.jpclett.2c00727
J. Phys. Chem. Lett. 2022, 13, 3937−3941

mechanism of the transition metal−LiH system on N_2 activation.

The $RuHN_2(LiH)_n^-$ (n = 0−2) complexes were generated via pulsed laser vaporization of the ruthenium−lithium hydride catalysts in a supersonic of helium gas and subsequently characterized with a coupled photoelectron velocity-map imaging spectrometer (see the Supporting Information for experimental details). The experimental photoelectron imaging spectra of $RuHN_2(LiH)_n^-$ (n = 0−2) recorded at 355 nm are shown in Figure 1. The reconstructed images (purple

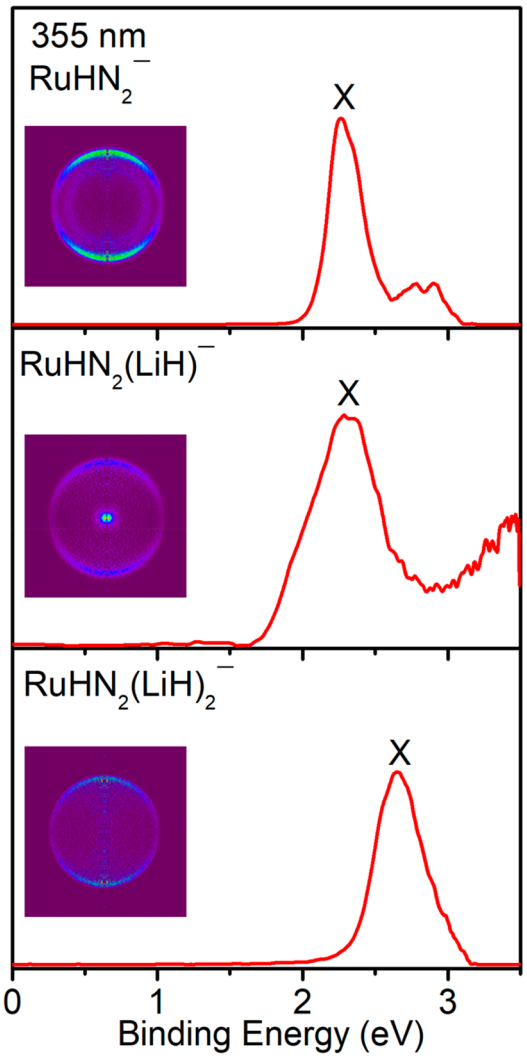

Figure 1. Photoelectron spectra of $RuHN_2(LiH)_n^-$ (n = 0−2) recorded at 355 nm (3.496 eV). Photoelectron images after inverse Abel transformation are embedded in the photoelectron spectra.

background) denote the central slice of the three-dimensional (3D) laboratory frame photoelectron distribution from its two-dimensional (2D) projection. The dominant main peak labeled with the letter X in each spectrum has a distinct band maximum, which directly determines the ground-state vertical detachment energy (VDE) values for n values of 0, 1, and 2 to be 2.27 ± 0.06, 2.29 ± 0.06, and 2.65 ± 0.04 eV, respectively (Table 1). The bands from the spectra without vibrational features prevent us from directly measuring the ground-state adiabatic detachment energies (ADEs), which can be alternatively estimated by drawing a straight line at the leading edge of peak X and then adding the instrumental resolution to the electron binding energy at the crossing point between the line and the x-axis. The ADE values of the ground states for the $RuHN_2(LiH)_n^-$ (n = 0−2) complexes were accordingly evaluated to be 2.09 ± 0.07, 2.13 ± 0.07, and 2.37 ± 0.05 eV, respectively (Table 1).

To assign the observed spectral features and identify the geometric and electronic structures of the low-lying isomers, quantum chemical calculations were performed for $RuHN_2(LiH)_n^-$ (n = 0−2) at the BP86/6-311+G(2d, 2p)/SDD level of theory (see the Supporting Information for computational details). Three types of structures are predicted for all of these complexes. The first type is that in which N_2 is bonded to the Ru atom in an end-on configuration (labeled nA). The second type is that in which N_2 is bonded to the Ru atom in a side-on configuration (labeled nB). The third type is that in which N_2 is completely cleaved (labeled nC). Optimized structures of the nA, nB, and nC isomers for $RuHN_2(LiH)_n^-$ (n = 0−2) are illustrated in Figure 2 and Figure S2. For the $RuHN_2^-$ complex, the thermodynamically most stable isomer is the end-on structure (0A) with a H atom and N_2 terminally bonded to the Ru atom from the opposite sides in a linear structure (Figure 2). The 0B structure with a side-on N_2 bonded to the Ru atom is 0.35 eV higher in energy than 0A. The 0C structure is 0.92 eV higher in energy than 0A, where the N≡N bond is completely cleaved. For the $RuHN_2(LiH)_n^-$ (n = 1 and 2) complexes, the nC structures are more stable than the nA and nB structures.

To clarify the possible structures that exist under the experimental conditions, the calculated VDE and ADE values for each structure are compared with the experimental values in Table 1. When n = 0, the calculated VDE and ADE values of the lowest-lying structure (0A) of 2.12 and 1.97 eV, respectively, are consistent with the experimental values (2.27 and 2.09 eV, respectively). The calculated VDE and ADE values of 0B (1.93 and 1.89 eV, respectively) and 0C (2.58 and 2.47 eV, respectively) are much smaller or larger than the experimental data. Similar to the n = 1 and 2 cases, the most stable 1C and 2C isomers are identified by their VDE and ADE values being closest to the experimental results. Additional evidence was obtained through comparing the theoretically calculated and experimentally obtained spectra, as shown in Figure S3. The consistent experimental and calculated spectra have indicated that the assignments of the 0A, 1C, and 2C structures are responsible for the experimental observations.

The potential energy profiles for the $RuN_2H(LiH)_n^-$ (n = 0−2) complexes calculated at the BP86/6-311+G(2d, 2p)/SDD level of theory are presented in Figure 3. When n = 0, it takes an energy barrier of 0.54 eV to convert the most stable linear 0A to form side-on structure 0B. During this process, the N atom of the end-on structure approaches the Ru atom to form the Ru−N bond, along with the elongation of the N−N bond from 1.16 to 1.19 Å. The isomerization from 0B to 0C involves the breaking of the N≡N bond, which needs to overcome a barrier of ≤3.43 eV. When n = 1, the isomerization from 1A to 1B goes through an energy barrier of 0.62 eV to form the side-on structure (1B) from the end-on structure (1A) with the N−N bond length increasing from 1.19 to 1.22 Å. Subsequently, the N−N bond length increases from 1.22 to 2.92 Å to form the 1C structure with a 3.30 eV barrier. When n = 2, the N−N bond length is increased from 1.18 to 1.23 Å with a 0.83 eV barrier from 2A to 2B. The N−N bond length

https://doi.org/10.1021/acs.jpclett.2c00727
J. Phys. Chem. Lett. 2022, 13, 3937−3941

Table 1. Comparison of Experimental VDE and ADE Values to BP86-Calculated Values of the Three Lowest-Energy Isomers for $RuHN_2(LiH)_n^-$ (n = 0−2)

			VDE (eV)		ADE (eV)	
cluster	isomer	relative energy (eV)	exptl[a]	calcd	exptl[a]	calcd
$RuHN_2^-$	0A	0	2.27(6)	2.12	2.09(7)	1.97
	0B	0.35		1.93		1.89
	0C	0.92		2.58		2.47
$RuHN_2(LiH)^-$	1A	0.18		1.55		1.34
	1B	0.50		1.36		1.24
	1C	0	2.29(6)	2.15	2.13(7)	2.00
$RuHN_2(LiH)_2^-$	2A	0.07		1.93		1.60
	2B	0.41		1.98		1.19
	2C	0	2.65(4)	2.58	2.37(5)	2.26

[a]Numbers in parentheses represent the uncertainty in the last digit.

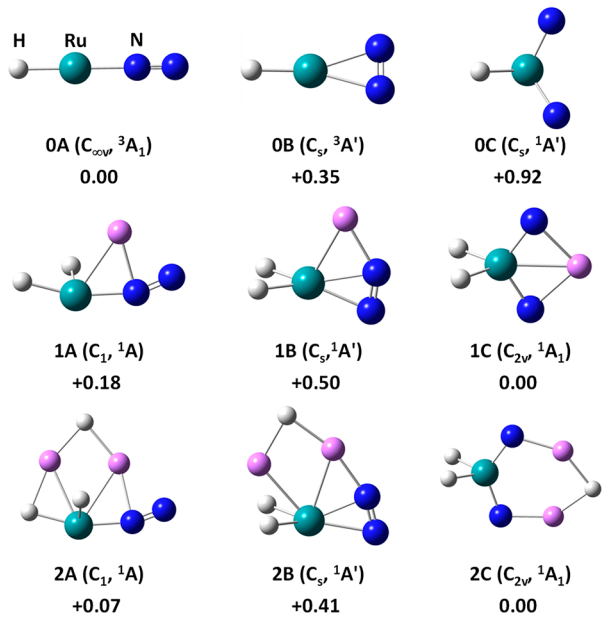

Figure 2. Ground-state structures and selected low-lying isomers of the $RuHN_2(LiH)_n^-$ (n = 0−2) anions (Ru, green; Li, purple; N, blue; H, white) calculated at the BP86/6-311+G(2d, 2p)/SDD level of theory. Relative energies are given in electronvolts after zero-point energy correction.

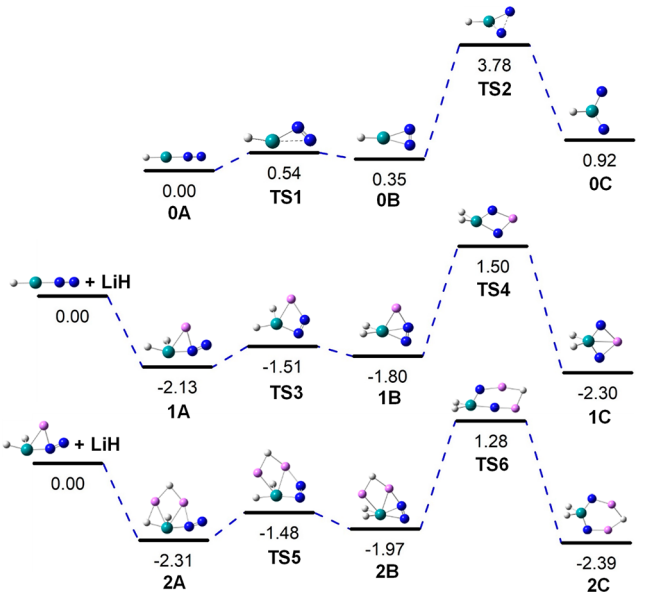

Figure 3. Potential energy surface for $RuHN_2(LiH)_n^-$ (n = 0−2) anions calculated at the BP86/6-311+G(2d, 2p)/SDD level of theory. Energies are given in electronvolts after zero-point energy correction.

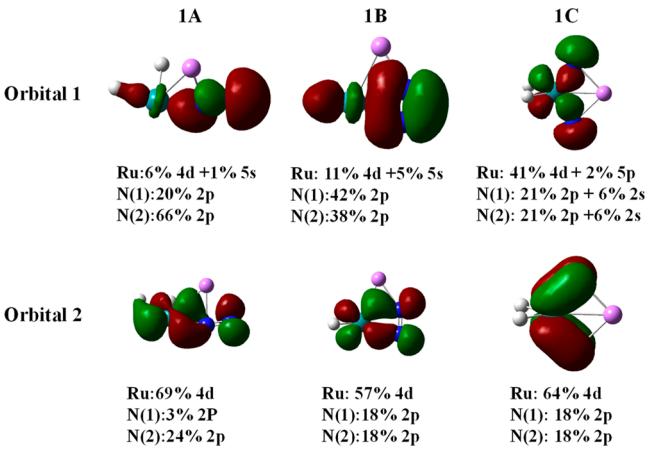

Figure 4. Schematic diagram of the bonding interactions between Ru and dinitrogen in the end-on-dinitrogen (left), side-on-dinitrogen (middle), and cleaved-dinitrogen structures of $RuHN_2(LiH)^-$.

continues to increase from 1.23 to 3.11 Å to form the 2C structure with a barrier of 3.25 eV. When n = 0−2, the initial step of the isomerization process from nA to nB can be viewed as the N of the end-on-dinitrogen structure getting closer to the Ru atom to form the Ru−N bond, along with the N−N bond being elongated. The following procedure can be regarded as the breaking of the Ru−Li bond and N≡N bond, along with the formation of the Li−N bond. In the illustrated transition states, the Li atom participates in the formation of the Ru−Li−N−N ring and promotes the appreciable reduction of the tension of the Ru−N−N ring. The energy barriers of TS2, TS4, and TS6 are calculated to be 3.43, 3.30, and 3.25 eV, respectively, which decreases with the cluster size. This suggests that the stepwise addition of LiH to $RuHN_2^-$ helps to lower the energy barrier of N≡N bond cleavage.

The bonding interactions between the Ru atom and dinitrogen in the end-on structure, side-on structure, and cleaved-dinitrogen structure for $RuHN_2(LiH)^-$ are shown in Figure 4. In the 1A structure, orbital 1 can be viewed as the donation of a σ orbital from N_2 into an empty 4d orbital of the Ru atom, while orbital 2 can be regarded as back-donation of a π orbital from the occupied 4d orbital of Ru to the antibonding

https://doi.org/10.1021/acs.jpclett.2c00727
J. Phys. Chem. Lett. 2022, 13, 3937−3941

Table 2. N−N Wiberg Bond Orders, Bond Lengths, and NBO Charges of the $RuHN_2(LiH)_n^-$ (n = 0−2) Species Calculated at the BP86 Level

			NBO charge							
	N−N bond order	N−N bond length	Ru	N(1)	N(2)	Li(1)	Li(2)	H(1)	H(2)	H(3)
0A	2.39	1.16	−0.12	−0.20	−0.25			−0.43		
0B	2.27	1.19	−0.18	−0.24	−0.24			−0.34		
0C	0.67	2.87	−0.01	−0.43	−0.43			−0.12		
1A	2.17	1.19	−0.67	−0.19	−0.37	0.46		−0.26	0.03	
1B	2.02	1.22	−0.76	−0.43	−0.22	0.50		−0.04	−0.04	
1C	0.6	2.92	−0.40	−0.68	−0.68	0.78		−0.01	−0.01	
2A	2.22	1.18	−0.69	−0.13	−0.32	0.50	0.50	−0.29	0.05	−0.60
2B	2.04	1.23	−0.71	−0.27	−0.31	0.55	0.55	−0.08	−0.08	−0.61
2C	0.61	3.11	−0.31	−0.74	−0.74	0.69	0.69	0.04	0.04	−0.67

π orbitals of N_2. In orbital 1 of the 1B structure, the π-bonding orbital of N_2 acts as the donor orbital. Orbital 2 involves back-donation of a π orbital from the occupied 4d orbital of Ru to the antibonding π orbitals of N_2. Previous studies pointed out that π back-donation would weaken the strong N≡N bond and was crucial for its further activation.[8] As both σ donation and π back-donation of the 1B structure can weaken the N≡N bond, while only π back-donation of the 1A structure weakens the N≡N bond, the side-on structure (1B) is reasonably supported to contain a more activated N_2 ligand than the end-on structure (1A) in accordance with the N−N bond order of 1B. With respect to 1C, orbitals 1 and 2 can be seen as the Ru−N σ orbital and Ru−N π orbital, respectively. The two orbitals jointly contribute to weaken the N≡N bond. Therefore, the 1C structure is more activated than the side-on structure, and the N≡N bond is completely cleaved. In the 1A−1B−1C isomerization process, the N−N bond is gradually elongated from 1.19 to 2.92 Å. The bonding interactions between the Ru atom and dinitrogen in these three types of structures of n = 0 and n = 2 are similar to that of the n = 1 case, which are displayed in Figures S4 and S5, respectively.

In the nA structures, the bonding interactions between Ru and dinitrogen contain both a σ bond and a π back-donation bond. The Wiberg bond orders of 1A and 2A are 2.17 and 2.22, respectively (Table 2), which are smaller than that of the 0A structure. This indicates that LiH contributes to dinitrogen activation. The nB structures include a π back-donation orbital and a σ orbital. The dinitrogen in the nB structures is more activated than in the nA structures. The Ru−N bond can be seen as a double bond. The N−N bond lengths of nC structures for n = 0−2 are 2.87, 2.92, and 3.11 Å, respectively, and the NBO charges of the N atom for nC (n = 0−2) structures are −0.43, −0.68, and −0.74, respectively. Therefore, the isomerization of nA, nB, and nC indicates that the LiH species in the transition metal catalysts effectively promotes the activation of N_2 via facilitating the energy-demanding N≡N cleavage process.

In summary, the $RuHN_2(LiH)_n^-$ (n = 0−2) complexes have been studied by combining mass-selected photoelectron velocity-map imaging spectroscopy and quantum chemical calculations. The most stable structure of $RuHN_2^-$ is determined to be a N_2-tagged complex. For $RuN_2H(LiH)_n^-$ (n = 1 and 2), the most stable structures are characterized to have N≡N bond-cleaved ring structures. These results show that the addition of LiH to RuH^- can cleave the N≡N bond. Theoretical analyses indicate that the synergy between Ru and LiH efficiently lowers the energy barrier of N≡N bond cleavage. These findings clarify the pivotal roles played by the LiH species in the transition metal catalysts for N_2 activation and also open new avenues for the development of related single-atom catalysts with isolated metal atoms dispersed on supports.

■ ASSOCIATED CONTENT

Supporting Information

The Supporting Information is available free of charge at https://pubs.acs.org/doi/10.1021/acs.jpclett.2c00727.

Experimental and theoretical methods, additional figures, and references (PDF)

Transparent Peer Review report available (PDF)

■ AUTHOR INFORMATION

Corresponding Authors

Ling Jiang − *State Key Laboratory of Molecular Reaction Dynamics, Dalian Institute of Chemical Physics, Chinese Academy of Sciences, Dalian 116023, China;* orcid.org/0000-0002-8485-8893; Email: ljiang@dicp.ac.cn

Hua Xie − *State Key Laboratory of Molecular Reaction Dynamics, Dalian Institute of Chemical Physics, Chinese Academy of Sciences, Dalian 116023, China;* orcid.org/0000-0003-2091-6457; Email: xiehua@dicp.ac.cn

Authors

Jumei Zhang − *State Key Laboratory of Molecular Reaction Dynamics, Dalian Institute of Chemical Physics, Chinese Academy of Sciences, Dalian 116023, China; School of Life Science, Ludong University, Yantai, Shandong 264025, China*

Gang Li − *State Key Laboratory of Molecular Reaction Dynamics, Dalian Institute of Chemical Physics, Chinese Academy of Sciences, Dalian 116023, China;* orcid.org/0000-0001-5984-111X

Jianping Guo − *Dalian National Laboratory for Clean Energy, Dalian Institute of Chemical Physics, Chinese Academy of Sciences, Dalian 116023, China;* orcid.org/0000-0002-0229-8555

Hongjun Fan − *State Key Laboratory of Molecular Reaction Dynamics, Dalian Institute of Chemical Physics, Chinese Academy of Sciences, Dalian 116023, China;* orcid.org/0000-0003-3406-6932

Ping Chen − *Dalian National Laboratory for Clean Energy, Dalian Institute of Chemical Physics, Chinese Academy of Sciences, Dalian 116023, China;* orcid.org/0000-0002-0625-0639

Complete contact information is available at: https://pubs.acs.org/10.1021/acs.jpclett.2c00727

https://doi.org/10.1021/acs.jpclett.2c00727
J. Phys. Chem. Lett. 2022, 13, 3937−3941

Notes

The authors declare no competing financial interest.

■ ACKNOWLEDGMENTS

The authors gratefully acknowledge the Dalian Coherent Light Source (DCLS) for support and assistance. This work was supported by the National Natural Science Foundation of China (Grants 21873097, 22103082, 92061203, and 21688102), the Youth Innovation Promotion Association of the Chinese Academy of Sciences (CAS) (2020187), the Strategic Priority Research Program of CAS (XDB17000000), CAS (GJJSTD20190002), and the K. C. Wong Education Foundation (GJTD-2018-06).

■ REFERENCES

(1) Guo, J. P.; Chen, P. Catalyst: NH_3 as an Energy Carrier. *Chem.* **2017**, *3*, 709−712.
(2) Erisman, J. W.; Sutton, M. A.; Galloway, J.; Klimont, Z.; Winiwarter, W. How a century of ammonia synthesis changed the world. *Nat. Geosci* **2008**, *1* (10), 636−639.
(3) Weare, W. W.; Dai, X.; Byrnes, M. J.; Chin, J. M.; Schrock, R. R.; Muller, P. Catalytic reduction of dinitrogen to ammonia at a single molybdenum center. *Proc. Natl. Acad. Sci. U.S.A.* **2006**, *103*, 17099−17106.
(4) Arashiba, K.; Miyake, Y.; Nishibayashi, Y. A molybdenum complex bearing PNP-type pincer ligands leads to the catalytic reduction of dinitrogen into ammonia. *Nat. Chem.* **2011**, *3*, 120−125.
(5) Anderson, J. S.; Rittle, J.; Peters, J. C. Catalytic conversion of nitrogen to ammonia by an iron model complex. *Nature* **2013**, *501*, 84−88.
(6) Yandulov, D. V.; Schrock, R. R. Catalytic reduction of dinitrogen to ammonia at a single molybdenum center. *Science* **2003**, *301*, 76−78.
(7) Wang, M.; Chu, L. Y.; Li, Z. Y.; Messinis, A. M.; Ding, Y. Q.; Hu, L. R.; Ma, J. B. Dinitrogen and Carbon Dioxide Activation to Form C− N Bonds at Room Temperature: A New Mechanism Revealed by Experimental and Theoretical Studies. *J. Phys. Chem. Lett.* **2021**, *12*, 3490−3496.
(8) Deng, G. H.; Pan, S.; Wang, G. J.; Zhao, L. L.; Zhou, M. F.; Frenking, G. Side-On Bonded Beryllium Dinitrogen Complexes. *Angew. Chem. Int. Ed* **2020**, *132*, 10690−10696.
(9) Jiang, G. D.; Li, Z. Y.; Mou, L. H.; He, S. G. Dual Iron Sites in Activation of N_2 by Iron − Sulfur Cluster Anions$Fe_5S_2^-$ and $Fe_5S_3^-$. *J. Phys. Chem. Lett.* **2021**, *12*, 9269−9274.
(10) Dahl, S.; Logadottir, A.; Jacobsen, C. J. H.; Nørskov, J. K. Electronic factors in catalysis: the volcano curve and the effect of promotion in catalytic ammonia synthesis. *Applied Catalysis A: General* **2001**, *222*, 19−29.
(11) Abild-Pedersen, F.; Greeley, J.; Studt, F.; Rossmeisl, J.; Munter, T. R.; Moses, P. G.; Skúlason, E.; Bligaard, T.; Nørskov, J. K. Scaling Properties of Adsorption Energies for Hydrogen-Containing Molecules on Transition-Metal Surfaces. *Phys. Rev. Lett.* **2007**, *99*, 016105.
(12) Logadottir, A.; Rod, T. H.; Nørskov, J. K.; Hammer, B.; Dahl, S.; Jacobsen, C. J. H. The Brønsted−Evans−Polanyi Relation and the Volcano Plot for Ammonia Synthesis over Transition Metal Catalysts. *J. Catal.* **2001**, *197*, 229−231.
(13) Wang, P. K.; Chang, F.; Gao, W. B.; Guo, J. P.; Wu, G. T.; He, T.; Chen, P. Breaking scaling relations to achieve low-temperature ammonia synthesis through LiH-mediated nitrogen transfer and hydrogenation. *Nat. Chem.* **2017**, *9* (1), 64−70.
(14) Pillai, E. D.; Jaeger, T. D.; Duncan, M. A. IR spectroscopy and density functional theory of small $V^+(N_2)_n$ complexes. *J. Phys. Chem. A* **2005**, *109* (16), 3521−3526.
(15) Pillai, E. D.; Jaeger, T. D.; Duncan, M. A. IR spectroscopy of $Nb^+(N_2)_n$ complexes: Coordination, structures, and spin states. *J. Am. Chem. Soc.* **2007**, *129* (8), 2297−2307.
(16) Xie, H.; Shi, L.; Xing, X. P.; Tang, Z. C. Infrared photodissociation spectroscopy of $M(N_2)_n^+$(M = Y, La, Ce; n = 7−8) in the gas phase. *Phys. Chem. Chem. Phys.* **2016**, *18* (6), 4444−4450.
(17) Brock, L. R.; Duncan, M. A. Photoionization spectroscopy of the In-N2 van der Waals complex. *J. Chem. Phys.* **1995**, *102* (24), 9498−9505.
(18) Hirotsu, M.; Fontaine, P. P.; Epshteyn, A.; Sita, L. R. Dinitrogen activation at ambient temperatures: New modes of H_2 and $PhSiH_3$ additions for an ″End-on-bridged″ Ta(IV)$_2$(μ-η^1:η^1-N_2) complex and for the bis(μ-nitrido) [Ta(V)(μ-N)]$_2$ product derived from facile N≡N bond cleavage. *J. Am. Chem. Soc.* **2007**, *129* (30), 9284−9285.
(19) Monillas, W. H.; Yap, G. P. A.; MacAdams, L. A.; Theopold, K. H. Binding and activation of small molecules by three-coordinate Cr(I). *J. Am. Chem. Soc.* **2007**, *129* (26), 8090−8091.
(20) Hagadorn, J. R.; Arnold, J. Low-valent chemistry of titanium benzamidinates leading to new Ti μ-N_2, μ-O, alkyl derivatives, and the cyclometalation of TMEDA. *J. Am. Chem. Soc.* **1996**, *118* (4), 893−894.
(21) Kilgore, U. J.; Yang, X. F.; Tomaszewski, J.; Huffman, J. C.; Mindiola, D. J. Activation of atmospheric nitrogen and azobenzene N≡N bond cleavage by a transient Nb(III) complex. *Inorg. Chem.* **2006**, *45* (26), 10712−10721.
(22) Gao, W. B.; Wang, P. K.; Guo, J. P.; Chang, F.; He, T.; Wang, Q. R.; Wu, G. T.; Chen, P. Barium Hydride-Mediated Nitrogen Transfer and Hydrogenation for Ammonia Synthesis: A Case Study of Cobalt. *Acs Catal.* **2017**, *7* (5), 3654−3661.
(23) Guo, J. P.; Chen, P. Interplay of Alkali, Transition Metals, Nitrogen, and Hydrogen in Ammonia Synthesis and Decomposition Reactions. *Acc. Chem. Res.* **2021**, *54*, 2434−2444.
(24) Ding, Y. Q.; Chen, Z. Y.; Li, Z. Y.; Cheng, X.; Wang, M.; Ma, J. B. Lithium-Assisted Dinitrogen Reduction Mediated by $Nb_2LiNO_{1-4}^-$ Cluster Anions: Electron Donors or Structural Units. *J. Phys. Chem. A* **2022**, *126*, 1511−1517.
(25) Chang, F.; Guan, Y. Q.; Chang, X. H.; Guo, J. P.; Wang, P. K.; Gao, W. B.; Wu, G. T.; Zheng, J.; Li, X. G.; Chen, P. Alkali and Alkaline Earth Hydrides-Driven N_2 Activation and Transformation over Mn Nitride Catalyst. *J. Am. Chem. Soc.* **2018**, *140* (44), 14799−14806.
(26) Wang, P.; Xie, H.; Guo, J.; Zhao, Z.; Kong, X.; Gao, W.; Chang, F.; He, T.; Wu, G.; Chen, M.; Jiang, L.; Chen, P. The Formation of Surface Lithium-Iron Ternary Hydride and its Function on Catalytic Ammonia Synthesis at Low Temperatures. *Angew. Chem., Int. Ed.* **2017**, *56* (30), 8716−8720.
(27) Wang, Q. R.; Pan, J.; Guo, J. P.; Hansen, H. A.; Xie, H.; Jiang, L.; Hua, L.; Li, H. Y.; Guan, Y. Q.; Wang, P. K.; Gao, W. B.; Liu, L.; Cao, H. J.; Xiong, Z. T.; Vegge, T.; Chen, P. Ternary ruthenium complex hydrides for ammonia synthesis via the associative mechanism. *Nat. Catal.* **2021**, *4*, 959−967.

https://doi.org/10.1021/acs.jpclett.2c00727
J. Phys. Chem. Lett. 2022, 13, 3937−3941